



Article

Planar Hall Effect and Magnetoresistance Effect in Pt/Tm₃Fe₅O₁₂ Bilayers at Low Temperature

Yukuai Liu ^{1,†} , Jingming Liang ^{2,†}, Zhiyong Xu ¹, Jiahui Li ¹, Junhao Ruan ¹, Sheung Mei Ng ², Chuanwei Huang ^{3,*} and Chi Wah Leung ^{2,*} 

¹ College of Electronic Information and Mechatronic Engineering, Zhaoqing University, Zhaoqing Road, Duanzhou District, Zhaoqing 526061, China; liuyukuai@zqu.edu.cn (Y.L.)

² Department of Applied Physics, The Hong Kong Polytechnic University, Hung Hom, Hong Kong, China

³ Shenzhen Key Laboratory of Special Functional Materials, Guangdong Provincial Key Laboratory of New Energy Materials Service Safety, College of Materials Science and Engineering, Shenzhen University, Shenzhen 518060, China

* Correspondence: cwhuang@szu.edu.cn (C.H.); dennis.leung@polyu.edu.hk (C.W.L.)

† These authors contributed equally to this work.

Abstract

Spin transport behaviors in heavy metal/ferromagnetic insulator (HM/FI) bilayers have attracted considerable attention due to various novel phenomena and applications in spintronic devices. Herein, we investigate the planar Hall effect (PHE) in Pt/Tm₃Fe₅O₁₂ (Pt/TmIG) heterostructures at low temperatures; moment switching in the ferrimagnetic insulator TmIG is detected by using electrical measurements. Double switching hysteresis PHE curves are found in Pt/TmIG bilayers, closely related to the magnetic moment of Tm³⁺ ions, which makes a key contribution to the total magnetic moment of TmIG film at low temperature. More importantly, a magnetoresistance (MR) curve with double switching is found, which has not been reported in this simple HM/FI bilayer, and the sign of this MR effect is sensitive to the angle between the magnetic field and current directions. Our findings of these effects in this HM/rare earth iron garnet (HM/REIG) bilayer provide insights into tuning the spin transport properties of HM/REIG by changing the rare earth.

Keywords: Tm₃Fe₅O₁₂ thin film; planar Hall effect; magnetoresistance; spintronic device



Academic Editor: Jonghwa Eom

Received: 17 July 2025

Revised: 28 July 2025

Accepted: 30 July 2025

Published: 31 July 2025

Citation: Liu, Y.; Liang, J.; Xu, Z.; Li, J.; Ruan, J.; Ng, S.M.; Huang, C.; Leung, C.W. Planar Hall Effect and Magnetoresistance Effect in Pt/Tm₃Fe₅O₁₂ Bilayers at Low Temperature. *Electronics* **2025**, *14*, 3060. <https://doi.org/10.3390/electronics14153060>

Copyright: © 2025 by the authors. Licensee MDPI, Basel, Switzerland. This article is an open access article distributed under the terms and conditions of the Creative Commons Attribution (CC BY) license (<https://creativecommons.org/licenses/by/4.0/>).

1. Introduction

The study of magnetization reversal processes using magnetotransport measurements lies at the heart of spintronics and has potential for applications in information technology and sensing [1,2]. Tunneling magnetoresistance (TMR), the anomalous Hall effect (AHE), and the planar Hall effect (PHE) are commonly used for detecting magnetization reversal and realizing highly sensitive sensors. As for the PHE, the resolution of the angle for detecting the direction of magnetization is about twice as good as that of MR [3], and it can be used as a magnetic sensor for applications like compasses with an angular resolution better than 0.5° [4,5].

The PHE in magnetic materials is due to the relative orientation of the current and the magnetization; thus, it can be used to investigate the magnetic switching and anisotropy of ferromagnetic materials [4,6–9]. The physical origin of PHE is closely linked to the spin-orbital coupling (SOC) effect [6]. In a simple model, the transverse and longitudinal resistances (R_{xy} and R_{xx} , respectively) are given by the following [6,10]:

$$R_{xy} = (R_{||} - R_{\perp}) \sin\gamma \cos\gamma \quad (1)$$

$$R_{xx} = R_{\perp} + (R_{||} - R_{\perp}) \cos^2\gamma \quad (2)$$

where $R_{||}$ and R_{\perp} are the resistances of the current parallel and perpendicular to the direction of the magnetization, and γ is the angle (in-plane) between the magnetization and current flow.

Apart from investigating the magnetization reversal in magnetic materials [4,6–8], the PHE has also become a powerful tool to detect the spin–orbital coupling in heavy metal/ferromagnetic metal (HM/FM) heterostructures [11–14], in which the current passing through HM/FM structures with a strong SOC effect offers a very efficient way to gauge the moment of ferromagnets. Recently, SOC effects in heavy metal/ferrimagnetic insulator (HM/FI) bilayers have also been found and attracted lots of attention [15–20], whereby spin Hall magnetoresistance (SMR) and spin current transport have been observed at the HM/FI interface. In prototypical HM/FI heterostructures such as Pt/Tm₃Fe₅O₁₂ (Pt/TmIG), while charge current cannot flow in the TmIG layer, the spin current generated by the spin Hall effect (SHE) in Pt can be transmitted across the Pt/TmIG interface, which is influenced by the magnetic property of the TmIG. Here, Tm³⁺ plays a key role in the total magnetic moment of TmIG at low temperatures, which shows obvious effects on the spin transport in Pt/TmIG heterostructures [21,22]. So far, reports on PHE in HM/FI bilayers are limited, and this method of detecting the SOC between HM and FI and the magnetization switching in the FI layer may help us observe new physical phenomena.

In the present work, the PHE in Pt/TmIG heterostructures is investigated, and the magnetic switching behaviors of TmIG films are detected through magnetotransport measurements. More importantly, a magnetoresistance (MR) curve with double switching is found in the Pt/TmIG bilayer. Temperature-dependent PHE and MR effects indicate that these unique behaviors are closely related to the magnetic moment of the Tm³⁺ sublattice, which clarifies the key role of this rare earth at low temperatures. Our findings show that the possible design of novel memories based on this MR curve with double switching in some simple HM/FI heterostructures would benefit applications in spintronic devices.

2. Experiment

2.1. Synthesis of Pt/TmIG Heterostructures

High-quality TmIG films (8 nm) were grown on (111)-orientated Gd₃Ga₅O₁₂ (GGG) substrates through pulsed laser deposition (PLD) at 710 °C and 100 mTorr. First, 5 nm of Pt with a Hall bar pattern (channel width: 160 μm; channel length: 500 μm) was deposited by rf sputtering through a stainless steel shadow mask. Details of deposition and structural characterization can be found in [19].

2.2. Transport Measurements of Pt/TmIG Heterostructures

All of the magnetotransport measurements were performed in a physical property measurement system (PPMS, Quantum Design) with an applied current of 100 μA. A schematic of the experimental configuration is shown in Figure 1a, where the current is applied along the x -axis and the angle γ denotes the direction of the (in-plane) applied magnetic field H relative to the x -axis. Two types of experiments were carried out. Firstly, field-dependent transport measurements were taken with H applied along with specific values of γ . Secondly, we fixed the magnitude of H , and the sample was rotated in both clockwise and counterclockwise directions.

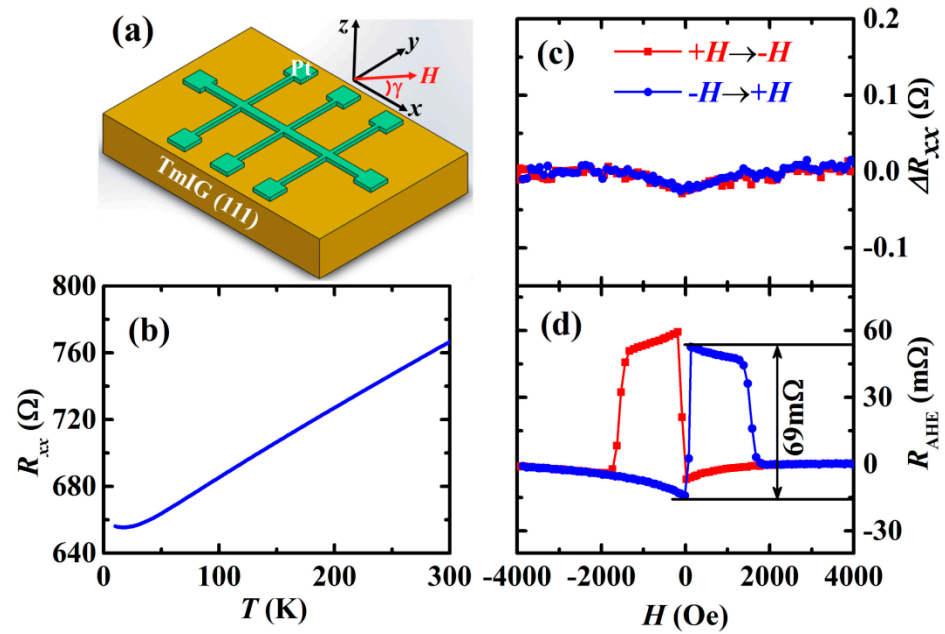


Figure 1. (a) Hall device schematic and the magnetotransport measurement setup, where the electric current is applied along the x -axis. (b) Temperature dependence curve of the R_{xx} . Magnetic field dependences of ΔR_{xx} (c) and R_{PHE} (d) at 10 K, and H is applied along the x -axis. Variation in R_{PHE} by about 69 mΩ is recorded in (d).

3. Results and Discussion

3.1. Magnetotransport of Pt/TmIG Heterostructures at 10 K

The Hall device schematic and the magnetotransport measurement setup are shown in Figure 1a. ΔR_{xx} of the Pt layer drops linearly with the decreasing temperature, indicating the metallic behavior, as shown in Figure 1b. And the resistance minimum at low temperatures is similar to previous reports of Pt grown on other garnet thin films [20,23]. In terms of magnetotransport measurements, when H is applied along the current direction (i.e., $\gamma = 0^\circ$), ΔR_{xx} vs. H shows a slight increase with the field (Figure 1c) and remains persistent at high field. Herein, ΔR_{xx} is defined as follows: $\Delta R_{xx} = [R_{xx}(H) - R_{xx}(H_{\max})]$, where $R_{xx}(H)$ and $R_{xx}(H_{\max})$ are the R_{xx} at H and the maximum applied field (4 kOe), respectively. As for the planar Hall resistance (R_{PHE}) in Figure 1d, a double switching loop is observed for $\gamma = 0^\circ$ after the linear background is subtracted. One can see from the results that the amplitude of planar Hall resistance (δR_{PHE}) is about 69 mΩ. The two abrupt switching events are typically correlated with magnetization switching in the ferromagnetic layer [6,7].

3.2. Angular Dependence of the Magnetotransport of Pt/TmIG Heterostructures

Figure 2 shows the γ -dependent magnetotransport behavior (ΔR_{xx} - H and R_{PHE} - H) of the Pt/TmIG bilayer at 10 K. From the in-plane angular dependent ΔR_{xx} - H curves (Figure 2a), it can be seen that for $\gamma = 30^\circ$ and 180° , the magnetoresistance effect is almost negligible. As for other angles, the ΔR_{xx} - H plots exhibit an MR curve with double switching, meaning the occurrence of ΔR_{xx} plateaus at intermediate H that are distinct from high field situations; the amplitude of R_{xx} variation (δR_{xx}) is almost constant (~ 0.16 to 0.18 Ω). We are not aware of reports about such an MR behavior in the HM/FI bilayer. For the PHE curves (Figure 2b), two switching loops are always observed at different values of γ , accompanied by variation in coercivity. This behavior is attributed to the magnetic anisotropy of the TmIG film [6,9]. The angular dependence of δR_{xx} is shown in Figure 3a. The sensitivity of δR_{xx} to γ , leading to both negative and positive MR effects, can be observed in this HM/FI

heterostructure. Moreover, the magnitude and sign of the δR_{PHE} are also dependent on γ . Figure 3b shows the γ dependence of δR_{PHE} , which decreases and changes sign around $\gamma = 30^\circ$ and then increases with γ and reaches $+69 \text{ m}\Omega$ at 180° . This MR effect with obvious positive and negative changes is very conducive to the design and application of new memory devices.

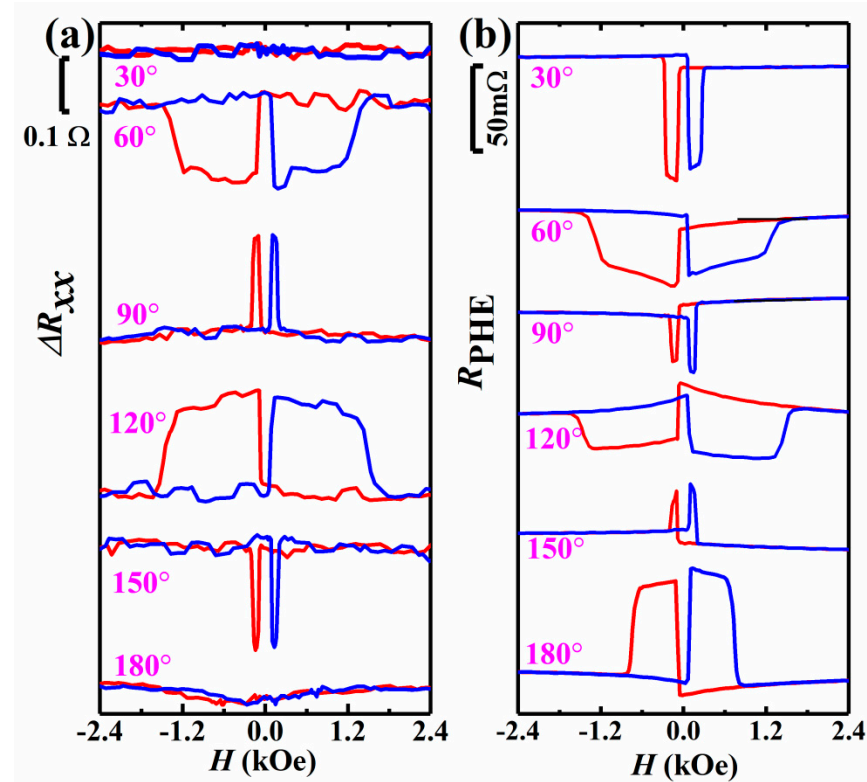


Figure 2. In-plane angular dependence of ΔR_{xx} - H (a) and R_{PHE} - H (b) loops at 10 K. The red and blue traces indicate different sweeping field directions (red: decreasing H ; blue: increasing H). The vertical scale bars for (a,b) are different due to drawing limitations.

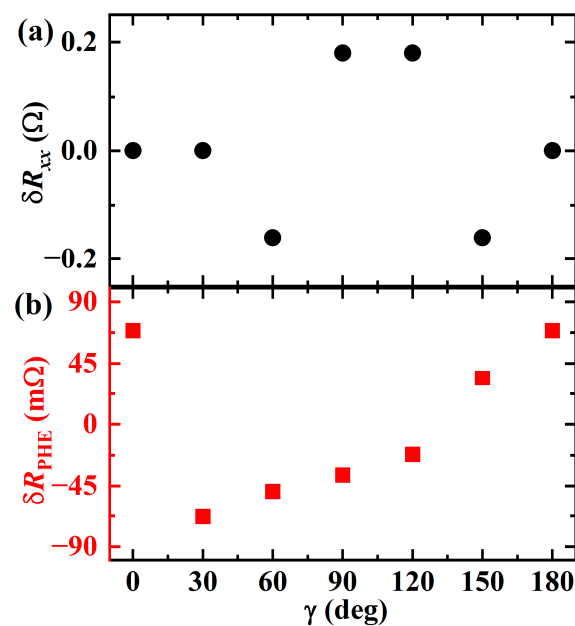


Figure 3. Angular dependences of δR_{xx} (a) and δR_{PHE} (b) obtained from PHE curves.

The dependences of ΔR_{xx} and R_{PHE} of the Pt/TmIG bilayer with γ at 10 K are plotted in Figure 4, with γ sweeping from 0° to 360° (black curves) and then back to 0° (red curves). At low field ($H = 300$ Oe), hysteresis with abrupt transitions is observed in ΔR_{xx} - γ and R_{PHE} - γ curves at $\gamma = 90^\circ$, 135° , 270° , and 315° due to the switching of magnetization between magnetic easy axes, indicating the presence of magnetic anisotropy in TmIG. In the TmIG structure, its magnetic moment consists of two Fe^{3+} sublattices and one Tm^{3+} sublattice [21,22]; thus, these transitions may originate from the magnetization switching of these magnetic sublattices. The angular dependence of the width of both hysteresis of ΔR_{xx} and R_{PHE} systematically decreases with increasing magnetic field and then disappears when H is up to about 1 T. At $H = 5$ T, both angular dependences of ΔR_{xx} and R_{PHE} show non-hysteresis behavior, and the maximum ΔR_{xx} is found at 0° and 180° , indicating that the resistance of the current parallel to the magnetic field (direction of the magnetization of TmIG) is larger than that of the current perpendicular to the magnetic field. While for R_{PHE} , it exhibits extrema for applied magnetic field orientations around 45° , 135° , 225° , and 315° , which is consistent with Equation (1).

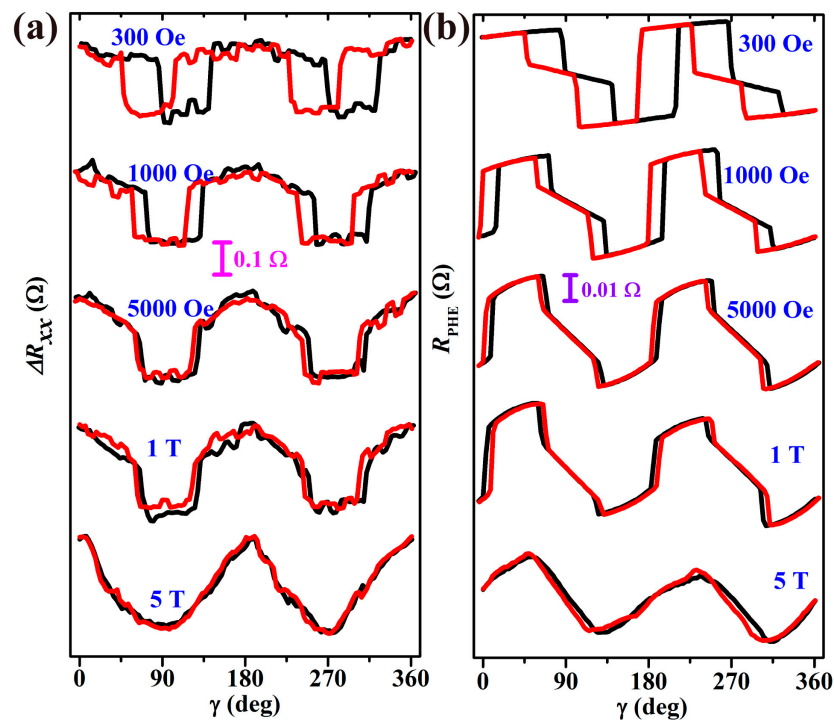


Figure 4. Angular dependence of ΔR_{xx} (a) and R_{PHE} (b) of Pt/TmIG heterostructures with a fixed magnitude of H at 10 K. The black traces have H sweeping from 0° to 360° , and the red traces represent the H sweeping direction from 360° to 0° .

As reported in ferromagnetic (Ga, Mn)As [6,24], Fe_3O_4 [25], manganite [7], and other ferromagnetic multilayers [3,4], PHE is closely linked to the in-plane magnetization vector, making it particularly suitable for studying in-plane magnetization switching processes in samples with weak magnetization signals. It is worth mentioning that when rare earth ion garnet (REIG) thin films are grown on paramagnetic substrates such as GGG, the colossal paramagnetic moment contribution [16,18–20,23] makes it difficult to separate the magnetization switching of the REIG films by traditional magnetic measurements. Meanwhile, as RE^{3+} makes a prominent contribution to the total moment of REIG [21,22], studies of temperature-dependent magnetization are of significance. Recent experiments have confirmed strong interface coupling between the spins of RE^{3+} and Fe^{3+} and conduction electrons of Pt in the Pt/REIG bilayer [26]. Therefore, based on the large SOC effect in Pt

and the spin current phenomenon in Pt/REIG heterostructures [16,18,20,23], it is possible to detect the magnetization switching behavior of REIG films by studying the PHE of Pt/REIG bilayers, which is confirmed by our present results.

The ΔR_{xx} - H curves in Figure 2 are similar to those observed in typical magnetic tunnel junctions, albeit in the absence of the tunneling device structure [27]. The anomalous switching behavior of the ΔR_{xx} - H curves in Figures 2 and 3 can be explained by a two-step sequence of magnetization, resulting from the magnetic structure of TmIG, where both Fe^{3+} and Tm^{3+} sublattices make contributions to the total magnetic moment of TmIG, and the Tm^{3+} sublattice moment plays the key role, especially at low temperatures [21].

To further study the PHE and MR effects in Pt/TmIG bilayers observed in Figures 2 and 3, we investigated their temperature dependences when $\gamma = 0^\circ$ and 90° , the results of which are shown in Figures 5 and 6, respectively. As for $\gamma = 0^\circ$ (Figure 5), the magnetoresistance effect is similar to that observed at 10 K (Figure 1c). For PHE, with increasing temperature, the hysteresis becomes narrower; in particular, the switching field at a high field range becomes smaller with increasing temperature, as shown in Figure 5a. When the temperature reaches above 60 K (Figure 5b), the switching loops disappear and the shape becomes butterfly-like. Therefore, this double switching behavior in Pt/TmIG devices is only observed at low temperatures.

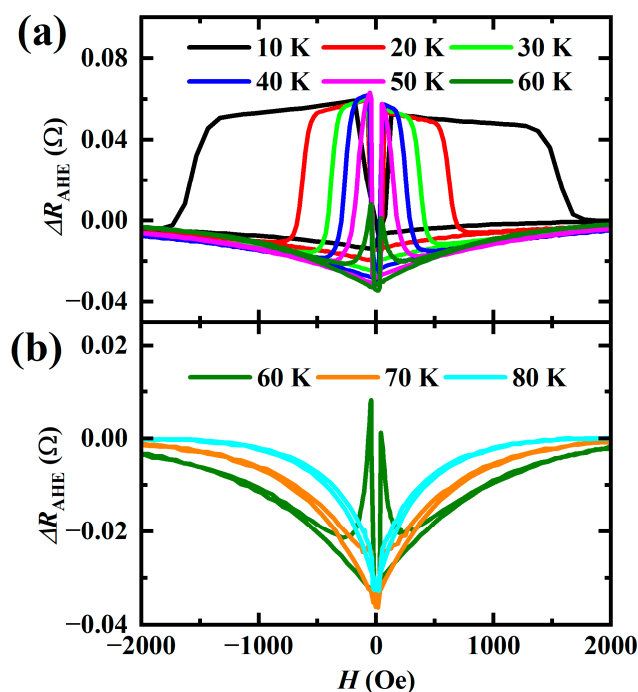


Figure 5. Temperature dependence of R_{PHE} at $\gamma = 0^\circ$: (a) below 60 K and (b) above 60 K.

While the Curie temperature of TmIG is about 550 K, [21] at low temperatures, Tm^{3+} makes an obvious contribution to the total moment of TmIG [21,22,28]. Bearing in mind that Tm exhibits a long-range magnetic order up to 51 K (antiferromagnetic) [29], in the low-temperature region, both Fe^{3+} and Tm^{3+} sublattices thus make contributions to the total magnetic moment of TmIG. The observed double hysteresis loops in Pt/TmIG heterostructures below 60 K are likely closely related to the magnetic properties of the Tm^{3+} sublattice.

As for $\gamma = 90^\circ$, the PHE and MR effects of Pt/TmIG show complex behavior (Figure 6). With the temperature increasing up to 60 K, the ΔR_{xx} - H curves still exhibit an MR curve with double switching (Figure 6a–e), similar to that observed in Figure 2a. When the temperature is above 60 K, the shape of ΔR_{xx} - H curves (Figure 6f–h) becomes butterfly-like.

like, which is similar to other Pt/ReIG bilayers [15]. These results further confirm that the magnetoresistance (MR) curve with double switching in Pt/TmIG only occurs at low temperatures, which likely results from the contribution of Tm^{3+} .

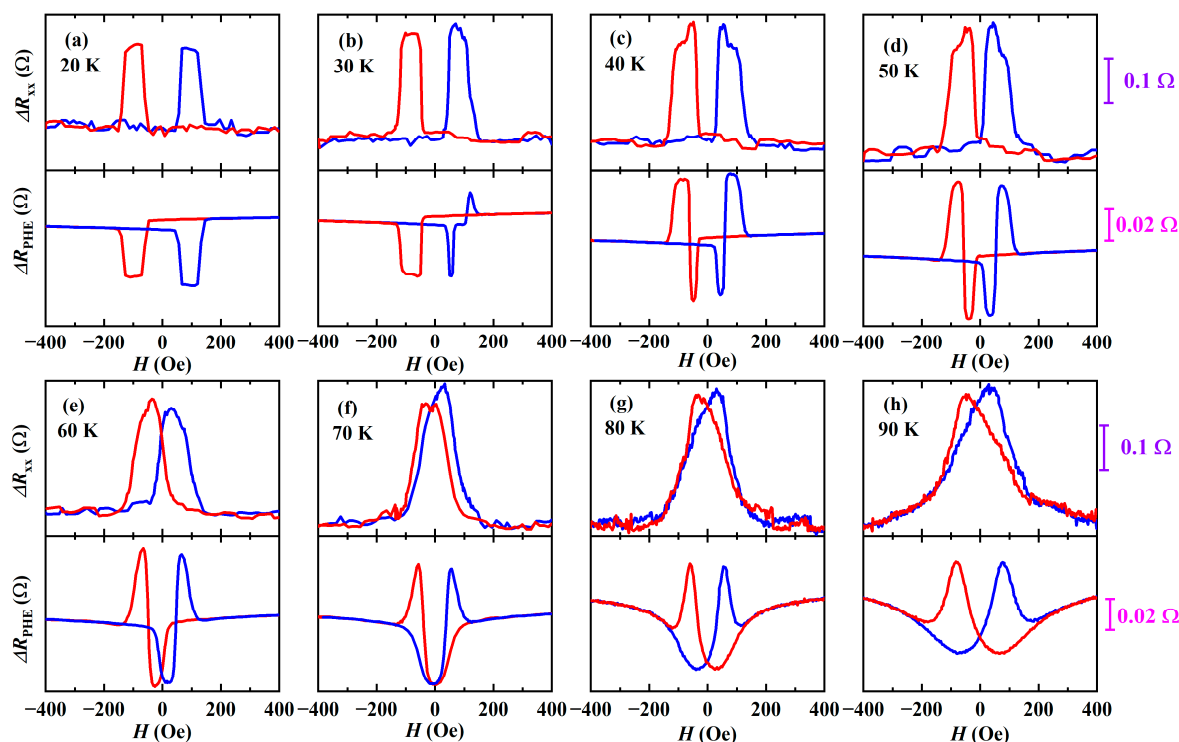


Figure 6. Temperature-dependent ΔR_{xx} - H and ΔR_{PHE} - H curves of Pt/TmIG heterostructures with $\gamma = 90^\circ$: (a) $T = 20$ K, (b) $T = 30$ K, (c) $T = 40$ K, (d) $T = 50$ K, (e) $T = 60$ K, (f) $T = 70$ K, (g) $T = 80$ K and (h) $T = 100$ K. In each panel, the upper (lower) plots show the magnetic field dependence of ΔR_{xx} (ΔR_{PHE}). Red and blue traces represent H sweeping from positive to negative and from negative to positive, respectively.

As for the magnetic field dependence of PHE, the ΔR_{PHE} - H curve shows up-switching apart from the two down-switching at 30 K (Figure 6b), which becomes more obvious with increasing temperatures (Figure 6c). It is worth noting that four switching instances are found between 40 K and 70 K, which have not been reported in other Pt/REIG systems. And with further increases in temperature, the ΔR_{PHE} - H curves show the butterfly-like shapes in Figure 6g,h, which are similar to the ΔR_{xx} - H curves.

In the Pt/TmIG heterostructure, TmIG exhibits ferrimagnetic properties but is highly insulating, while Pt possesses a strong SOC that can be used to detect the magnetization switching of the adjacent ferrimagnets [11–14]. Therefore, it is reasonable to attribute these special switching loops in ΔR_{PHE} - H and ΔR_{xx} - H curves at low temperatures (Figures 4 and 5) to the complex magnetic structure of TmIG [21,22]. The magnetic structure of TmIG consists of two sublattices of Fe^{3+} occupying octahedral and tetrahedral sites, where they couple antiferromagnetically, and one Tm^{3+} sublattice where Tm^{3+} ions occupy the dodecahedral positions [30]. At high temperatures, iron sublattices dominate, while at low temperatures, the Tm^{3+} sublattice becomes increasingly relevant [21,22]. The reported temperature-dependent magnetization of TmIG film indicates that the minimum magnetization is observed near 50 K [31], which results from the interactions of Fe^{3+} sublattices and Tm^{3+} sublattices. Obviously, the limitation for this magnetoresistance (MR) curve with double switching in the Pt/TmIG bilayer is that its working temperature is far below the actual temperature, which may be improved by constructing a heterostructure TmIG with other iron garnets or designing spin valves by using iron garnets [32].

On the other hand, people have found the spin Hall magnetoresistance effect in Pt/TmIG heterostructures [19,33], where, in these HM/FMI bilayers, people can simply measure the resistance of the adjacent HM layer to detect the magnetization direction of the FMI layer [34]. In our present work, we measure the MR effect as the magnetic field is rotated in the film plane; the magnetoresistance curve with double switching is related to the magnetization switching of Tm^{3+} and Fe^{3+} sublattices in TmIG. Therefore, the MR effect with double switching in the Pt/TmIG heterostructure should be induced by the SMR.

4. Conclusions

In summary, the planar Hall and magnetoresistance effects in Pt/TmIG heterostructures at low temperatures are systematically studied. The double switching behavior of PHE is found, which is closely related to the magnetic moment switching of TmIG. A magnetoresistance curve with double switching is observed in magnetoresistance measurements of Pt/TmIG heterostructures. The observation of PHE and MR effects in Pt/TmIG enables systematic investigation of the in-plane magnetic anisotropy, especially in some REIG thin films, which have complicated magnetic moment switching behavior. Furthermore, our study provides an electrical measurement to study the magnetic switching behavior of the Tm^{3+} sublattice, which can also be used to investigate other iron garnets or magnetic insulators. Thus, our results indicate that rare earths can play an important role in spin transport behavior in Pt/REIG heterostructures.

Author Contributions: Conceptualization, Y.L.; methodology, Y.L. and J.L. (Jingming Liang); data curation, Y.L., Z.X. and J.L. (Jiahui Li); investigation, J.R. and S.M.N.; writing—original draft preparation, Y.L., J.L. (Jingming Liang) and C.W.L.; supervision, C.H. and C.W.L.; writing—review and editing, Y.L., J.L. (Jingming Liang), C.H. and C.W.L. All authors have read and agreed to the published version of the manuscript.

Funding: This work was supported by the Hong Kong Research Grant Council (PolyU 15302320), the Hong Kong Polytechnic University (ZVWC, CD6U, WZA1), and Shenzhen Science and Technology Program (20220809153419002).

Data Availability Statement: The original contributions presented in this study are included in the article.

Conflicts of Interest: The authors declare no conflicts of interest.

References

1. Zutic, I.; Fabian, J.; Sarma, S.D. Spintronics: Fundamentals and Applications. *Rev. Mod. Phys.* **2004**, *76*, 323. [\[CrossRef\]](#)
2. Fukami, S.; Ohno, H.; Zhang, C.; DuttaGupta, S.; Kurenkov, A. Magnetization Switching by Spin–Orbit Torque in an Antiferromagnet–Ferromagnet Bilayer System. *Nat. Mater.* **2016**, *15*, 535. [\[CrossRef\]](#)
3. Ko, T.W.; Park, B.K.; Lee, J.H.; Rhie, K.; Kim, M.Y.; Rhee, J.R. Planar Hall Effect of Glass/Fe 70 Å/[Co 21Å/Cu 25Å]₂₀ Multilayers. *J. Magn. Magn. Mater.* **1999**, *198*, 64–66. [\[CrossRef\]](#)
4. Adeyeye, A.O.; Win, M.T.; Tan, T.A.; Chong, G.S.; Ng, V.; Low, T.S. Planar Hall Effect and Magnetoresistance in Co/Cu Multilayer Films. *Sens. Actuators A Phys.* **2004**, *116*, 95–102. [\[CrossRef\]](#)
5. Montaigne Fo Schuhl, A.; Dau, F.N.V.; Encinas, A. Development of Magnetoresistive Sensors Based on Planar Hall Effect for Applications to Microcompass. *Sens. Actuators A Phys.* **2000**, *81*, 324. [\[CrossRef\]](#)
6. Tang, H.X.; Kawakami, R.K.; Awschalom, D.D.; Roukes, M.L. Giant Planar Hall Effect in Epitaxial (Ga, Mn) as Devices. *Phys. Rev. Lett.* **2003**, *90*, 107201. [\[CrossRef\]](#)
7. Bason, Y.; Klein, L.; Yau, J.B.; Hong, X.; Ahn, C.H. Giant Planar Hall Effect in Colossal Magnetoresistive La_{0.84}Sr_{0.16}MnO₃ Thin Films. *Appl. Phys. Lett.* **2004**, *84*, 2593–2595. [\[CrossRef\]](#)
8. Seemann, K.M.; Freimuth, F.; Zhang, H.; Blugel, S.; Mokrousov, Y.; Burgler, D.E.; Schneider, C.M. Origin of the Planar Hall Effect in Nanocrystalline Co₆₀Fe₂₀B₂₀. *Phys. Rev. Lett.* **2011**, *107*, 086603. [\[CrossRef\]](#)
9. Shin, J.; Kim, S.; Lee, S.; Yoo, T.; Lee, H.; Khym, S.; Lee, S.; Liu, X.; Furdyna, J.K. Asymmetry in the Angular Dependence of the Switching Field of Gamnas Film. *J. Appl. Phys.* **2011**, *109*, 07C308. [\[CrossRef\]](#)

10. Thompson, D.A.; Romankiw, L.T.; Mayadas, A.F. Thin Film Magnetoresistors in Memory, Storage, and Related Application. *IEEE Trans. Magn.* **1975**, *11*, 1039. [\[CrossRef\]](#)
11. Garello, K.; Miron, I.M.; Avci, C.O.; Freimuth, F.; Mokrousov, Y.; Blugel, S.; Auffret, S.; Boulle, O.; Gaudin, G.; Gambardella, P. Symmetry and Magnitude of Spin—Orbit Torques in Ferromagnetic Heterostructures. *Nat. Nanotechnol.* **2013**, *8*, 587. [\[CrossRef\]](#)
12. Fan, X.; Wu, J.; Chen, Y.; Jerry, M.J.; Zhang, H.; Xiao, J.Q. Observation of the Nonlocal Spin-Orbital Effective Field. *Nat. Commun.* **2013**, *4*, 1799. [\[CrossRef\]](#) [\[PubMed\]](#)
13. Yokouchi, T.; Kanazawa, N.; Tsukazaki, A.; Kozuka, Y.; Kikkawa, A.; Taguchi, Y.; Kawasaki, M.; Ichikawa, M.; Kagawa, F.; Tokura, Y. Formation of in-Plane Skyrmions in Epitaxial MnSi Thin Films as Revealed by Planar Hall Effect. *J. Phys. Soc. Jpn.* **2015**, *84*, 104708. [\[CrossRef\]](#)
14. Kong, W.J.; Ji, Y.R.; Zhang, X.; Wu, H.; Zhang, Q.T.; Yuan, Z.H.; Wan, C.H.; Han, X.F.; Yu, T.; Fukuda, K.; et al. Field-Free Spin Hall Effect Driven Magnetization Switching in Pd/Co/IrMn Exchange Coupling System. *Appl. Phys. Lett.* **2016**, *109*, 132402. [\[CrossRef\]](#)
15. Nakayama, H.; Althammer, M.; Chen, Y.T.; Uchida, K.; Kajiwara, Y.; Kikuchi, D.; Ohtani, T.; Geprags, S.; Opel, M.; Takahashi, S.; et al. Spin Hall Magnetoresistance Induced by a Nonequilibrium Proximity Effect. *Phys. Rev. Lett.* **2013**, *110*, 206601. [\[CrossRef\]](#)
16. Wang, H.L.; Du, C.H.; Pu, Y.; Adur, R.; Hammel, P.C.; Yang, F.Y. Scaling of Spin Hall Angle in 3d, 4d, and 5d Metals from Y3Fe5O12/Metal Spin Pumping. *Phys. Rev. Lett.* **2014**, *112*, 197201. [\[CrossRef\]](#) [\[PubMed\]](#)
17. Aldosary, M.; Li, J.; Tang, C.; Xu, Y.; Zheng, J.-G.; Bozhilov, K.N.; Shi, J. Platinum/Yttrium Iron Garnet Inverted Structures for Spin Current Transport. *Appl. Phys. Lett.* **2016**, *108*, 242401. [\[CrossRef\]](#)
18. Li, J.; Xu, Y.; Aldosary, M.; Tang, C.; Lin, Z.; Zhang, S.; Lake, R.; Shi, J. Observation of Magnon-Mediated Current Drag in Pt/Yttrium Iron Garnet/Pt(Ta) Trilayers. *Nat. Commun.* **2016**, *7*, 10858. [\[CrossRef\]](#)
19. Avci, C.O.; Quindeau, A.; Pai, C.F.; Mann, M.; Caretta, L.; Tang, A.S.; Onbasli, M.C.; Ross, C.A.; Beach, G.S. Current-Induced Switching in a Magnetic Insulator. *Nat. Mater.* **2017**, *16*, 309–314. [\[CrossRef\]](#)
20. Liu, Y.K.; Wong, H.F.; Lam, K.K.; Chan, K.H.; Mak, C.L.; Leung, C.W. Anomalous Hall Effect in Pt/Tb3Fe5O12 Heterostructure: Effect of Compensation Point. *J. Magn. Magn. Mater.* **2018**, *468*, 235–240. [\[CrossRef\]](#)
21. Geller, S.; Remeika, J.P.; Sherwood, R.C.; Williams, H.J.; Espinosa, G.P. Magnetic Study of the Heavier Rare-Earth Iron Garnets. *Phys. Rev.* **1965**, *137*, A1034–A1038. [\[CrossRef\]](#)
22. Lehmann-Szweykowska, A.; Wigen, P.E.; Kowalewski, L.; Kaczmarek, M.M.; Mitchell, T.B. Orbital Effects in Magnetic Dynamics of Thulium Iron Garnets. *Phys. Rev. B* **1988**, *37*, 459–466. [\[CrossRef\]](#)
23. Lu, Y.M.; Choi, Y.; Ortega, C.M.; Cheng, X.M.; Cai, J.W.; Huang, S.Y.; Sun, L.; Chien, C.L. Pt Magnetic Polarization on Y3Fe5O12 and Magnetotransport Characteristics. *Phys. Rev. Lett.* **2013**, *110*, 147207. [\[CrossRef\]](#)
24. Shin, D.Y.; Chung, S.J.; Lee, S.; Liu, X.; Furdyna, J.K. Temperature Dependence of Magnetic Anisotropy in Ferromagnetic (Ga,Mn)As Films: Investigation by the Planar Hall Effect. *Phys. Rev. B* **2007**, *76*, 035327. [\[CrossRef\]](#)
25. Fernández-Pacheco, A.; De Teresa, J.M.; Orna, J.; Morellón, L.; Algarabel, P.A.; Pardo, J.A.; Ibarra, M.R.; Magen, C.; Snoeck, E. Giant Planar Hall Effect in Epitaxial Fe3O4 Thin Films and Its Temperature Dependence. *Phys. Rev. B* **2008**, *78*, 212402. [\[CrossRef\]](#)
26. Geprags, S.; Kehlberger, A.; Della Coletta, F.; Qiu, Z.; Guo, E.J.; Schulz, T.; Mix, C.; Meyer, S.; Kamra, A.; Althammer, M.; et al. Origin of the Spin Seebeck Effect in Compensated Ferrimagnets. *Nat. Commun.* **2016**, *7*, 10452. [\[CrossRef\]](#) [\[PubMed\]](#)
27. Miao, G.-X.; Münzenberg, M.; Moodera, J.S. Tunneling Path toward Spintronics. *Rep. Prog. Phys.* **2011**, *74*, 036501. [\[CrossRef\]](#)
28. Dionne, G.F.; Tumelty, P.F. Molecular-Field Coefficients of Tm3Fe5O12. *J. Appl. Phys.* **1979**, *50*, 8257–8258. [\[CrossRef\]](#)
29. Davis, D.D.; Bozorth, R.M. Magnetic Properties of Thulium Metal. *Phys. Rev.* **1960**, *118*, 1543–1545. [\[CrossRef\]](#)
30. Bernasconi, J.; Kuse, D. Canted Spin Phase in Gadolinium Iron Garnet. *Phys. Rev. B* **1971**, *3*, 811–815. [\[CrossRef\]](#)
31. Soares, C.C.; Mori, T.J.A.; Béron, F.; Moodera, J.S.; Cezar, J.C.; Brandão, J.; Vilela, G. Compensation-Like Temperature and Spin-Flip Switch in Strained Thulium Iron Garnet Thin Films: Tuning Sublattice Interactions for Ferrimagnetic Spintronics†. *ACS Appl. Nano Mater.* **2025**, *8*, 14567–14575. [\[CrossRef\]](#)
32. Damerio, S.; Sunil, A.; Janus, W.; Mehraeen, M.; Zhang, S.S.L.; Avci, C.O. Magnetoresistive Detection of Perpendicular Switching in a Magnetic Insulator. *Commun. Phys.* **2024**, *7*, 114. [\[CrossRef\]](#)
33. Nunley, T.N.; Guo, S.; Chang, L.-J.; Lujan, D.; Choe, J.; Lee, S.-F.; Yang, F.; Li, X. Quantifying Spin Hall Topological Hall Effect in Ultrathin Tm3Fe5O12/Pt Bilayers. *Phys. Rev. B* **2022**, *106*, 014415. [\[CrossRef\]](#)
34. Althammer, M.; Meyer, S.; Nakayama, H.; Schreier, M.; Altmannshofer, S.; Weiler, M.; Huebl, H.; Geprags, S.; Opel, M.; Gross, R.; et al. Quantitative Study of the Spin Hall Magnetoresistance in Ferromagnetic Insulator/Normal Metal Hybrids. *Phys. Rev. B* **2013**, *87*, 224401. [\[CrossRef\]](#)

Disclaimer/Publisher’s Note: The statements, opinions and data contained in all publications are solely those of the individual author(s) and contributor(s) and not of MDPI and/or the editor(s). MDPI and/or the editor(s) disclaim responsibility for any injury to people or property resulting from any ideas, methods, instructions or products referred to in the content.